Dark State Concentration Dependent Emission and Dynamics of CdSe Nanoplatelet Exciton-Polaritons

Woo Je Chang,[†,‡] Hongfei Zeng,[¶,‡] Connor K. Terry Weatherly,[§,‡] Justin Provazza,[§] Pufan Liu,[†] Emily A. Weiss,[§] Nathaniel P. Stern,[*,¶] and Roel Tempelaar[*,§]

†*Department of Materials Science and Engineering, Northwestern University, Evanston, Illinois 60208-3113, USA.*

‡*These authors contributed equally to this work*

¶*Department of Physics and Astronomy, Northwestern University, Evanston, Illinois 60208-3113, USA.*

§*Department of Chemistry, Northwestern University, Evanston, Illinois 60208-3113, USA.*

E-mail: n-stern@northwestern.edu; roel.tempelaar@northwestern.edu

Abstract

The recent surge of interest in polaritons has prompted fundamental questions about the role of dark states in strong light-matter coupling phenomena. Here, we systematically vary the relative number of dark state polaritons by controlling the number of stacked CdSe nanoplatelets confined in a Fabry-Pérot cavity. We find the emission spectrum to change significantly with an increasing number of nanoplatelets, with a gradual shift of the dominant emission intensity from the lower polariton branch to a manifold of dark states. Through accompanying calculations based on a kinetic model, this shift

is rationalized by an entropic trapping of excitations by the dark state manifold, while a weak dark state dispersion due to local disorder explains their non-zero emission. Our results point towards the relevance of the dark state concentration to the optical and dynamical properties of cavity-embedded quantum emitters with ramifications for Bose-Einstein condensate formation, polariton lasing, polariton-based quantum transduction schemes, and polariton chemistry.

Keywords

Polaritons, CdSe Nanoplatelets, Dark States, Optical Cavity, Kinetic Model, Quantum Emitters

Spectroscopy has long served as a tool for studying the properties of matter by perturbing atoms, molecules, or materials with radiation and measuring their response. Going beyond the perturbative regime, however, light-matter interactions can act as a means for manipulating the states of matter, enabled by "strong coupling" for which such interactions outcompete radiative and nonradiative damping.[1,2] Under strong coupling, quantized optical modes hybridize with matter-based quantum states producing half-light-half-matter excitations called "polaritons", which manifest as a Rabi splitting of optical resonances into an upper polariton (UP) and a lower polariton (LP) peak.[3] This opens up new opportunities for fundamental science and technology, examples of which include chemical control,[3–6] Bose-Einstein condensation,[7–9] polariton lasing,[10–13] and quantum transduction schemes.[14–17]

The strong coupling regime is accessible by reducing the optical mode volume and increasing the quality factor of the interacting electromagnetic field through the use of optical resonators such as cavities and plasmonic structures.[18,19] Under ultra-low mode volume conditions, strong coupling invoking single quantum emitters (matter-based constituents) can

be realized.[20,21] Alternatively, light-matter coupling can be amplified more easily by invoking a large number of quantum emitters, which is readily implemented using Fabry-Pérot (FP) cavities. However, distinct for such collective strong coupling is the formation of a manifold of $N-1$ optically-dark states energetically located between the UP and LP peaks,[4,22,23] where N is the number of quantum emitters. Such dark states are delocalized over multiple quantum emitters yet do not appreciably hybridize with the optical modes of the cavity,[24,25] and as such do not assume properties expected from single emitter polaritons. Moreover, with increasing N, dark states are believed to act as a thermodynamic reservoir that dominate the excited-state properties and dynamics of the matter-cavity system and mitigate many of the favorable effects of strong coupling.[26]

Unfortunately, dark states contribute negligibly to common spectroscopic techniques based on reflectance or transmission measurements due to their minimal hybridization with the cavity modes, and as a result, the fate of excitations under strong coupling is challenging to experimentally study. Early studies on dark states have resorted to pump probe and two-dimensional infrared spectroscopy[27,28] through which relaxation rates from the UP and LP states into the manifold of dark states have been determined. Alternatively, a means to directly access the dark state manifold is provided by off-resonant pumping, early implementations of which have involved cavity-embedded J-aggregates.[29,30] Recently, off-resonant pumping has been applied to cavity-embedded cadmium selenide (CdSe) nanoplatelets (NPLs),[31,32] where subsequent detection of emission unveiled the importance of phonons in mediating polariton transitions.[31] These advances notwithstanding, the systematic study of dark states remains in its infancy.

In this work, we demonstrate a modulation of excited state dynamics and emissive properties through a systematic increase of the dark state concentration, which to our knowledge has not been previously observed. This is accomplished by strong coupling of the excitonic states of CdSe NPLs to the modes of a FP cavity.[31,33–35] Due to the large transition dipole strength of the NPLs, strong coupling can be reached without needing to form a

large manifold of dark states, unlike weak quantum emitters such as molecules that require high concentrations to achieve strong coupling.[36,37] By means of a stacking of NPLs through layer-by-layer deposition, we increase the number of quantum emitters, and consequently the dark state concentration. Upon off-resonant pumping, radical changes are observed for the emission intensity ratio of the LP and a higher energy feature consisting of the UP and dark state manifold. Good agreement with kinetic modeling reveals that these changes reflect a concentration-dependent trapping of excitations in the dark state manifold from which emission is enabled by local static disorder. These results suggest avenues for optimizing polariton emission by balancing bright and dark state contributions under collective strong coupling through control of quantum emitter concentration.

Results and Discussion

Cavity Fabrication and Polariton Characterization

The CdSe NPLs were synthesized following the procedure presented by VanOrman *et al.* and had a thickness dimension of 5.5 CdSe unit cells.[38] To prepare the cavity structure shown in Figure 1a, an 80 nm thick Ag layer was thermally evaporated onto a Si substrate, followed by a 35 - 50 nm thick Al_2O_3 passivation layer applied by atomic layer deposition, where the thickness was dependent on the number of stacked NPLs. The sample was then submerged, Al_2O_3 side up, into a small amount of acetonitrile (an NPL antisolvent) followed by suspension of a thin layer of an NPL-in-hexane colloid onto the acetonitrile.[39] An optimized concentration of the NPL-in-hexane colloid allowed single NPLs to deposit on the top of the acetonitrile. The acetonitrile was then pipetted out such that the NPLs were left on the substrate (Figure S1). The microscopic morphology of the deposited NPLs was shown to produce a compact structure, with the NPLs dominantly having a face-down orientation (Figure S2). This face-down orientation guarantees the emission originated from only in-plane dipole components, which rules out spot-to-spot intensity variations due to orien-

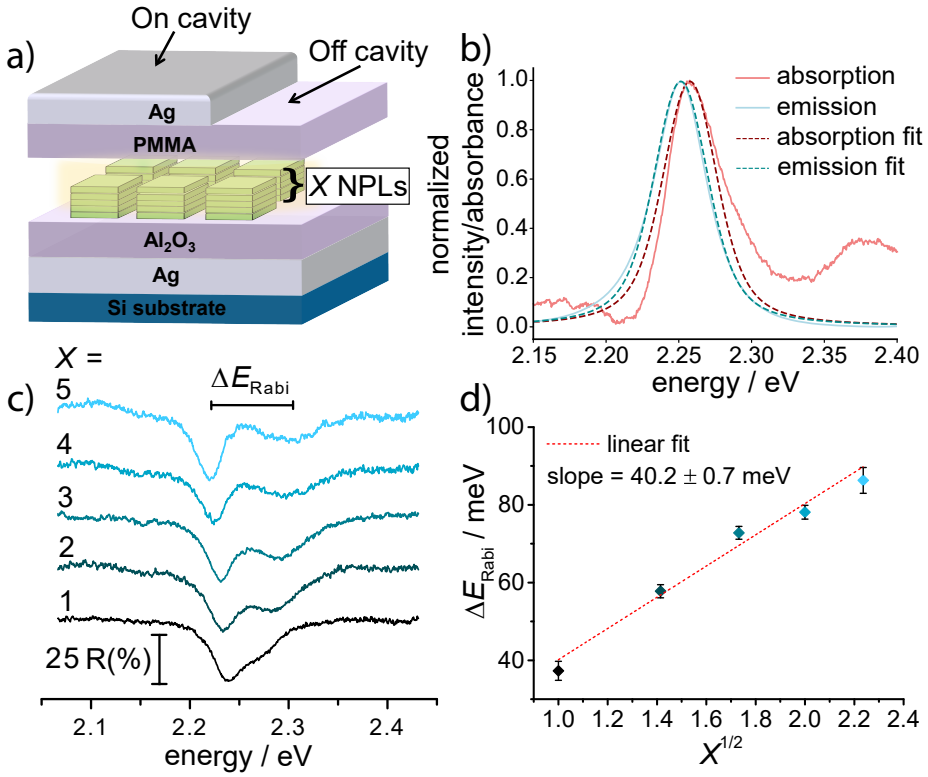

Figure 1: (a) Schematic of the FP cavity constructed with a CdSe NPL film and two Ag mirrors. A small sample area was not covered with the top Ag layer and was used for measuring the optical properties of the stacked NPLs when not coupled to the cavity mode, denoted as "off cavity". (b) Absorption (red) and emission (light blue) spectra of CdSe NPLs in the "off cavity" region. (c) Reflectance spectra of the NPL-cavity system as a function of the number of stacked NPLs, X. All data are at the zero detuning angle where the cavity photon and NPL exciton energy are equal. ΔE_{Rabi} denotes the Rabi splitting between the upper and lower polariton peaks. (d) ΔE_{Rabi} at zero detuning as a function of X. The Rabi splitting follows a linear scaling with $X^{1/2}$. Transverse electric (TE) polarized light was used in all measurements.

tation inconsistencies.[40] By repeating this process X amount of times, varying numbers of NPLs were stacked on top of one another (Figure 1a). The resulting NPL film was topped with an additional polymethyl methacrylate (PMMA) layer having a controlled thickness between 48-60 nm by means of spin-coating. To finalize the cavity structure, we thermally deposited a 60 nm Ag layer on top of the PMMA layer. To maintain a constant cavity thickness under variations in X, the concomitant increase in the NPL film thickness was compensated for by decreasing the thickness of the PMMA and Al_2O_3 layers.

We utilized a Fourier-plane spectroscopic technique (Figure S4) to study angle-dependent reflectance spectra for varying X in the cavity region. Shown in Figure 1c, are reflectance spectra recorded at the detection angle θ where polaritonic resonance occurs, i.e., where $\delta E = \hbar\Omega_{\mathrm{cav}}(\theta) - E_{\mathrm{exc}} = 0$. Here, E_{exc} is the exciton transition energy and $\Omega_{\mathrm{cav}}(\theta)$ is the frequency of the cavity mode. The dependence of the Ω_{cav} on θ is governed by Eq. S1 and for notational convenience, the dependence is dropped throughout the rest of this work. For each value of X, two dips were observed, which correspond to the UP and LP states. Note that there is no angle dependence of the bare NPL film in the "off cavity" region (Figure S6).

For a system with N degenerate quantum emitters (in this case NPLs) identically coupled to a cavity mode, the energy of the UP and LP states are given by

$$E_{\mathrm{UP/LP}} = \frac{1}{2}(E_{\mathrm{exc}} + \hbar\Omega_{\mathrm{cav}} \pm \sqrt{4Ng_0^2 + (\delta E)^2}) \tag{1}$$

where E_{UP} (corresponding to $+$) and E_{LP} (corresponding to $-$) are the energies of the UP and LP, respectively, and g_0 is the effective cavity coupling strength of a single emitter. At $\delta E = 0$, the Rabi splitting is

$$\Delta E_{\mathrm{Rabi}} = E_{\mathrm{UP}} - E_{\mathrm{LP}} = 2g_0\sqrt{N} = 2g_0\sqrt{\alpha X} \tag{2}$$

with α being the average number of NPLs per deposited layer. By fitting two Lorentzian functions to the reflectance spectra shown in Figure 1c, ΔE_{Rabi} was determined for each X

value. We note that Eq. 1 does not account for homogeneous broadening occurring in optical measurements. This broadening can cause the apparent UP and LP peak positions observed in reflectance measurements to differ from the actual polariton energies due to peak overlap. By fitting Lorentzian functions to the reflectance data in Figure 1c, we can determine the true UP and LP peak positions, validating our use of Eq. 1.

Figure 1d shows that ΔE_{Rabi} increases linearly with $X^{1/2}$, as predicted by Eq. 2. This demonstrates that the number of stacked NPLs scales as the concentration of cavity-coupled NPLs, with each deposited layer contributing an approximately equal number of cavity coupled NPLs, and that the coupling constant does not vary across stacked NPLs. In Figure 1d, the averaged values and error bars were determined from measurements at three different spots on two different samples for each value of X (Figures S7, and S8).

Figure 1 also shows the strong coupling regime is reached for each X value measured. The strong coupling condition is given by[2]

$$\Delta E_{\mathrm{Rabi}} > \Gamma_{\mathrm{cav}}/2 + \Gamma_{\mathrm{exc}}/2, \tag{3}$$

where Γ_{exc} and Γ_{cav} denote the homogeneous linewidths of the exciton and cavity mode, respectively. As mentioned, the absorption and emission measurements of the bare NPLs yielded $\Gamma_{\mathrm{exc}} = 23$ meV. Here, Γ_{cav} was determined from NPL cavities that were constructed with cavity modes significantly red detuned from the exciton transition, such that polariton formation was minimal, yielding $\Gamma_{\mathrm{cav}} = 32$ meV (Figure S5). Based on these values, Eq. 3 predicts that the strong coupling criterion is given by $\Delta E_{\mathrm{Rabi}} > 28$ meV. From Figure 1d, it follows that the strong coupling regime is reached for all values of X.

Dark-State Concentration Dependent Cavity Emission

The reflectance measurements primarily probe the cavity modes. As such, they inform on polaritons, as manifested by the UP and LP dips in the spectra shown in Figure 1c, but

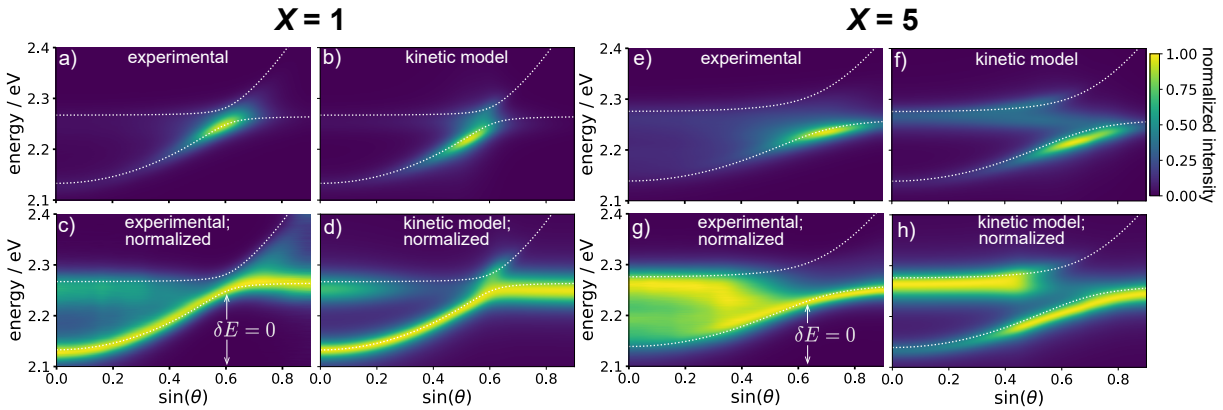

Figure 2: (a) Experimental and (b) calculated angle-dependent emission for $X = 1$ within an optical cavity. (c) and (d) are the same spectra as (a) and (b) but normalized at each value of $\sin(\theta)$. (e) Experimental and (f) calculated angle-dependent emission for $X = 5$ within an optical cavity. (g) and (h) are the same spectra as (e) and (f) but normalized at each value of $\sin(\theta)$. The white dashed lines show the UP and LP branches of Eq. 1 fit to the emission measurements in (c) for $X = 1$ and (g) for $X = 5$.

provide little information on the manifold of dark states. On the other hand, matter-based excitations project predominantly onto the manifold of dark states. To interrogate the latter, we generated matter-based photo-excitations by using a 473 nm (2.62 eV) continuous-wave laser to off-resonantly pump the cavity system, populating high-lying excited states in the NPLs that quickly relax into exciton-polariton. The cavity emission generated by such exciton-polaritons was then recorded. It is important to note that the polariton eigenstates are the same in both the reflectance and emission measurements. To optimally compare our results, the same location was probed in both measurements for a given cavity system.

Figure 2a presents angle-resolved emission measurements for $X = 1$, while analogs for $X = 5$ are presented in Figure 2e. The white dashed lines indicate corresponding fits of the UP and LP branches to the Jaynes-Cummings model, which are also compared to the reflectance data in Figure S7. Consistent with earlier observations by Qiu *et al.*,[31] the strongest emission intensity is seen to occur around $\delta E = 0$ meV, and to originate predominantly from the LP branch. Relative intensity variations render it difficult to analyze the emission spectra for detection-angles where $\delta E \neq 0$, which shows comparatively much weaker emission. To better analyze emission across all angles, we normalized spectra at each

angle to their respective highest intensity values. The result is shown in Figure 2c for $X = 1$ and in Figure 2g for $X = 5$ (emission spectra for $X = 2$, 3, and 4 are shown in Figures S9, S10 and S11, respectively). Clear variations in the normalized emission lineshape are seen across different values of X, especially for $\delta E < 0$ (red-detuned cavity). For $X = 1$, emission occurs predominantly from the LP branch at all detection angles. However, for $X = 5$, emission occurs predominantly at energies close to the UP branch when $\delta E < 0$. When $\delta E > 0$, weak emission is observed from the UP branch for $X = 1$, but not for $X = 5$. These differences in emission with varying NPL concentration cannot be understood solely from an energetic standpoint. Rather, they require a dynamical description of the polariton system driven by an off-resonant pumping. Accordingly, we constructed a kinetic model to describe such relaxation dynamics, as detailed below. Figures 2b and 2d show the calculated emission spectrum resulting from this model for $X = 1$ and Figures 2f and 2h show the equivalent for $X = 5$. Both show strong qualitative agreement with experiment and capture the increase in emission occurring near the UP branch.

Explaining Relaxation Dynamics Using a Kinetic Model

In order to account for the dynamics that give rise to the experimental emission spectra shown in Figure 2, we detailed the possible transitions that can occur in the system during off-resonant pumping, shown in Figure 3. This pumping populates high-lying excited states of the NPLs that quickly relax to band-edge excitons, which are superpositions of exciton-polariton eigenstates when coupled to a cavity. These states may delocalize over neighboring ground state NPLs through cavity-mediated coupling, forming a manifold of dark states along with the UP and LP states. The dark states have a large excitonic component, as a result of which high-lying excited states will dominantly relax into them (bold purple arrow in Figure 3), as previously shown by Qiu *et al.*[31] Figure 3 also shows the energetic dispersion of the dark states due to local static disorder of the NPLs causing them to slightly mix with the cavity mode. This allows for emission from all exciton-polariton states including dark states

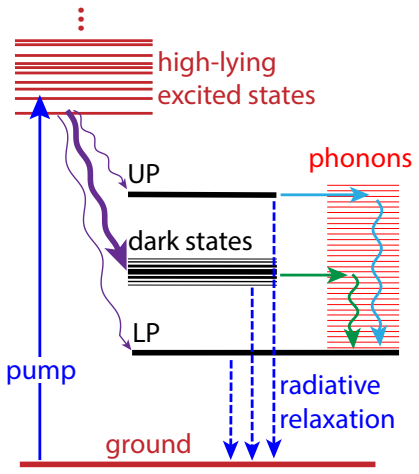

Figure 3: Jablonski diagram showing the radiative and non-radiative transitions that give rise to the emission spectra shown in Figure 2. Off-resonant pumping of the system into high-lying excited states is shown by the solid blue arrow; wavy arrows indicate non-radiative relaxation; blue dashed arrows indicate radiative relaxation that gives rise to emission.

(blue dashed arrows in Figure 3). Along with emission, transitions between polariton states occur, mediated by exciton-phonon coupling, as also shown in Figure 3. This allows the population to relax towards the LP state. Despite this relaxation, a large number of dark states will potentially act as a thermodynamic reservoir which can trap population. Such population trapping is consistent with the emission maximum occurring near the UP branch for $X = 5$ when $\delta E < 0$ (Figure 2g). For $X = 1$, the number of dark states is decreased and less population trapping is expected to occur, resulting in less dark state emission, which is observed in Figure 2c.

Our kinetic model (Section 8 of the Supporting Information) is based on a Holstein-type Hamiltonian including linear coupling of the excitonic states to a 200 cm^{-1} longitudinal optical (LO) phonon mode[41,42] as well as to a cavity mode. The exciton-phonon coupling strength in our model—characterized by the displacement (D) between the potential energy surface (PES) minima of the exciton and ground state—was taken as a free parameter used to match the calculated polariton emission to the experimental emission. It was kept the

same for each X value used and all other parameters were experimentally determined. We found $D = 25.4$ Å to give the closest match to the experimental emission measurements. This may be compared to $D = 7.0$ Å determined for the 200 cm^{-1} LO phonon mode in resonance Raman measurements of CdSe NPLs.[42] Other phonon modes[41] are likely to also generate coupling between polariton states, accounting for the overestimated D value required to accurately model the experimental emission. In our kinetic model, we also included variations in excitonic energies across NPLs in order to account for local static disorder giving rise to the inhomogeneous broadening of the exciton (Figure 1b). We took each exciton to couple equally to the cavity mode by an amount g_0, since most of the NPLs have uniform orientation (Figure S2) and likely do not involve appreciable spot-to-spot variations in the coupling strength.

In the polariton basis (Section 8 of the Supporting Information), the Hamiltonian corresponding to the system as described above is given by

$$\hat{H} = \sum_{\alpha=0}^{N} E_\alpha \left|\alpha\right\rangle \left\langle\alpha\right| + \sum_{n=1}^{N} \left[\frac{\hat{p}_n^2}{2} + \frac{1}{2}\omega_0^2 \hat{x}_n^2 - \omega_0^2 D \hat{x}_n \sum_{\alpha,\beta=0}^{N} M_{\alpha\beta}^{(n)} \left|\alpha\right\rangle \left\langle\beta\right| \right], \tag{4}$$

where $\hat{x}_n$ and $\hat{p}_n$ are the mass weighted position and momentum operators, respectively, of the phonon mode on the nth NPL with frequency, ω_0, and D is the displacement of the phononic PES minimum between the excitonic ground and lowest excited state (heavy-hole exciton). Furthermore, $|\alpha\rangle$ and $|\beta\rangle$ are the exciton-polariton states with energies E_α and E_β, respectively, and $M_{\alpha\beta}^{(n)} = \langle\alpha|e_n, 0\rangle \langle e_n, 0|\beta\rangle$ is the associated transformation matrix element involving the $|e_n, 0\rangle$ state, representing the nth NPL in its lowest excited state with no cavity photon present. It is apparent in Eq. 4 that the NPL exciton-phonon interaction results in an off diagonal coupling between polariton states, with the coupling strength between $|\alpha\rangle$ and $|\beta\rangle$ depending on both the displacement of the PES minimum, D, as well as the projection of $|\alpha\rangle$ and $|\beta\rangle$ onto each NPL exciton. From this off diagonal coupling, we derived transition rates between polariton states using a non-Condon type rate expression employing

the truncated Wigner approximation[43–45] (Section 8 of the Supporting Information).

Using the calculated rates between polariton states, the dynamics of the system are determined by the Pauli master equation

$$\dot{P}_\alpha = \sum_{\alpha \neq \beta} (w_{\alpha\beta} P_\beta - w_{\beta\alpha} P_\alpha), \tag{5}$$

where P_α and P_β are the occupancies of $|\alpha\rangle$ and $|\beta\rangle$, respectively. The transition rate from the ground state into each polariton state was determined by taking γ_{exc} to be the two-step excitation rate (outside of the cavity) from the ground state into an exciton state, $|e_n, 0\rangle$, which occurs through the manifold of high-lying excited states. This excitation process has equal probability to excite any NPL, and therefore, creates a mixed state with a uniform probability distribution between each exciton state. Within the cavity, relaxation from high-lying excited states into the manifold of polariton states will be proportional to the projection of this mixed state onto each polariton state. Accordingly, the excitation rate from the ground state into $|\alpha\rangle$ is given by

$$w_{g\alpha}^{\text{exc}} = \langle \alpha | \hat{U}^\dagger \hat{\rho}_0 \hat{U} | \alpha \rangle \, \Gamma_{\text{exc}}/2, \tag{6}$$

where

$$\hat{\rho}_0 = \frac{1}{N} \sum_{n=1}^{N} |e_n, 0\rangle \langle e_n, 0| , \tag{7}$$

and where $\hat{U}$ is the unitary transformation matrix composed of the eigenvectors of $\hat{H}_{\text{pol}}$ given by Eq. S3. Each exciton state $|e_n, 0\rangle$ has a large projection onto the manifold of dispersed dark states and a small projection onto the UP and LP states. This causes the relaxation from the high-lying excited states into the manifold of dispersed dark states to dominate over relaxation into the UP and LP states, as shown by the purple arrows in Figure 4a.

Radiative relaxation *via* leaky cavity luminescence[46] occurs from all polariton states that have a non-zero projection onto the cavity photon mode, $|g, 1\rangle$. Following the work of Qiu

et al.,[31] the radiative relaxation rate from $|\alpha\rangle$ is given by

$$w_{\alpha g}^{\mathrm{rad}} = |\langle \alpha | g, 1 \rangle|^2 \Gamma_{\mathrm{cav}}/2. \tag{8}$$

As before, $\Gamma_{\mathrm{cav}} = 32$ meV.

With local static disorder included in the model, the manifold of dark states becomes energetically dispersed and each dark state attains a small projection onto the cavity mode. This allows emission to occur from the dark states, as shown by the blue arrows in Figure 4a, yielding a feature in between the UP and LP peaks to be observed in the emission spectrum.[47] In this work, we sampled exciton energies from a Gaussian distribution based on the inhomogeneous broadening of the "off-cavity" NPL emission in Figure 1b (13 meV).

Due to continuous population of the polariton manifold from the ground state and radiative relaxation back into the ground state, the system quickly reaches a dynamic equilibrium. Equilibrium populations are calculated by diagonalizing the total rate matrix of the system. These populations are taken as the diagonal elements of the density operator at dynamic equilibrium ($\hat{\rho}(t_{\mathrm{eq}})$) and the emission spectra are then calculated using

$$I(\omega) = \sum_{\alpha} \frac{\rho_\alpha |\langle \alpha | g, 1 \rangle|^2 \Gamma_\alpha/2}{(\omega - E_\alpha/\hbar)^2 + (\Gamma_\alpha/2)^2}. \tag{9}$$

Here, $\rho_\alpha = \langle \alpha | \hat{\rho}(t_{\mathrm{eq}}) | \alpha \rangle$, ω is the frequency of the emitted radiation, and

$$\Gamma_\alpha/2 = |\langle \alpha | g, 1 \rangle|^2 \Gamma_{\mathrm{cav}}/2 + \sum_{n}^{N} |\langle \alpha | e_n, 0 \rangle|^2 \Gamma_{\mathrm{hom}}/2. \tag{10}$$

According to Eq. 9, the emission intensity from a certain polariton state is the product of both the occupancy of that state and the projection of that state onto the cavity mode.

Figures 4a and 4b schematically show the mechanism underlying the emission shift from the LP to the manifold of dark states with increasing NPL concentration when $\delta E < 0$. At low NPL concentrations (Figure 4a), the phonon mediated transitions allow population

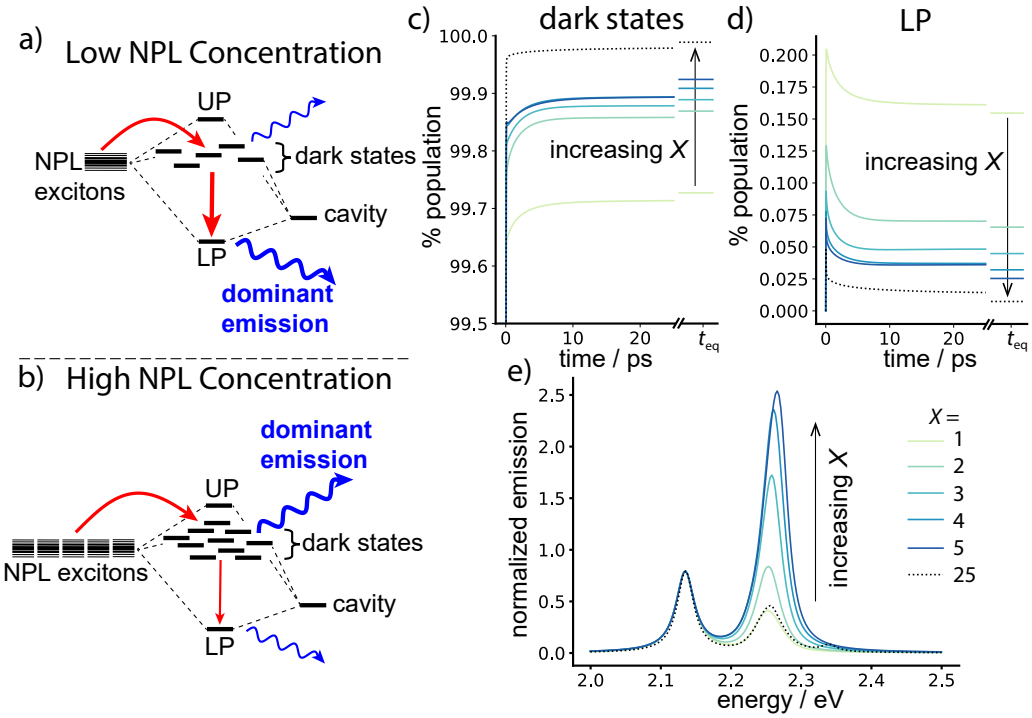

Figure 4: (a) Schematic showing an energy diagram and the emission process when a low concentration of NPLs are present in the cavity. The limited number of dispersed dark states allows for effective relaxation into the LP state, resulting in a predominant emission from there. (b) Same schematic but for a high concentration of NPLs present in the cavity. The entropic trapping of population in the dispersed dark states inhibits relaxation to the LP state (thin red arrow) resulting in a predominant emission from the former. Calculated population of (c) the dispersed dark states and (d) the LP state as a function of time during off-resonant pumping for different numbers of NPLs. The dark state population was computed as the sum of the population of each individual dark state. (e) Calculated emission spectra as a function of the number of NPLs in the cavity. The bare cavity energy was chosen so that the LP emission peak resides at 2.125 eV for all numbers of NPLs considered. All spectra were calculated at zero degree detection angle as taken from Figure 2.

to relax to the LP, which has a large projection onto the cavity mode, causing its emission intensity to be greater than that of the dark state manifold. At high NPL concentrations (Figure 4c), the increased number of dark sates will cause polaritons to have an enhanced likelihood to transfer between the different dark states instead of relaxing into the LP state. Additionally, the large number of dark states will increase the probability for polaritons to fluctuate from the LP into the manifold of dark states, shifting the population balance further to the dark state manifold. The large population of dark states then makes up for the small projection of individual dark states onto the cavity mode, causing dominant emission from the dark state manifold at higher NPL concentrations.

We used the kinetic model described above to calculate the time dependent population of the different polariton states during off-resonant excitation. Accompanying emission spectra calculations showed excellent agreement with experimental results, as seen in Figure 2. We also modeled the kinetics for varying number of NPLs with the cavity mode tuned such that the LP peak appeared at 2.125 eV for each run (Figure 4c-e). The total population of all dark states (Figure 4c) shows an increase at t_{eq} with increasing number of NPLs. On the other hand, the LP population shows a concomitant decrease (Figure 4d). These data substantiate that concentration-dependent population trapping by dark states causes the shift in emission intensity with increasing number of NPLs. The emission spectra corresponding to these calculations are shown in Figure 4e, and have all been normalized to the LP peak, so that the ratio of the dark states peak to the LP peak can easily be compared. In our calculations, $X = 1$ was represented by 26 NPLs, which can be considered an effective number of NPLs involved in the polaritonic states (limited due to the optical wavelength and the possibility of spatially proximate polaritons). From 26 through 130 ($X = 5$) NPLs, the emission intensity from the UP is convoluted with dark state emission. At these concentrations the UP is effectively part of the manifold of dark states but has an increased photonic component. Since it is close in energy to the manifold of dark states, thermal fluctuations drive population into it, as was observed recently by Amin *et al.*,[48] and as such it contributes to the emission

from the manifold of dark states. At 650 NPLs ($X = 25$; black dashed line), the collective coupling is large enough that an energetic gap between the dark states and the UP arises and thermal fluctuations are less likely to drive population into the UP, causing its emission intensity to be low.

Conclusion

Observing the effect of dark states on polariton dynamics has historically been a challenging task. This work demonstrates that the response of cavity emission to systematic changes in the cavity coupled emitter concentration provides important insights into the role of dark states on polariton dynamics and the corresponding emission spectrum. By increasing the number of CdSe NPLs coupled to a FP cavity, we observed emission, induced by off-resonant photo-excitation, to be increasingly dominated by the dark state manifold. A kinetic model, involving phonon-mediated relaxation between polariton states, indicated that this change in the emission profile is the result of an entropic trapping effect. This demonstrates that in collectively coupled systems the emitter concentration and cavity frequency can be tuned to manipulate the rate of relaxation to the LP. As a result, in the study of polaritons, more than the two extremes—the single emitter and thermodynamic limit of dark states—must be considered. Rather, there exist regimes of dark state concentration with significantly varying properties. These regimes open future opportunities for the manipulation of matter by coupling it to optical cavities and aid in establishing design principles for polariton-based optical devices such as lasing,[49] condensates,[9] or chemical reactors.[50] By recognizing these regimes, our study helps predict how collective coupling, disorder, and exciton-phonon coupling impact the dynamics of dark states and how they serve as a channel for population transfer between bright and dark polaritonic states.

Supporting Information

The supporting information includes further synthetic details and a characterization of the CdSe NPLs, the fabrication of the NPL-cavity device, a schematic of the NPL film formation procedure, scanning tunneling electron microscopy (STEM) images of a single the CdSe NPL film layer showing their typical face down orientation within the cavity, analysis of the nanostructral uniformity of the NPLs from STEM images, details and a schematic of the Fourier spectroscopic set-up used for reflectance and emission measurements, details on the determination of the cavity linewidth, the angle dependence of the bare exciton reflectance and emission profiles, angle resolved reflectance measurements for $X = 1$ through 5, duplicate reflactance measurements, and comparison of experimental and simulated angle dependent emission for $X = 2$ through 4. It also includes the polaritonic Hamiltonian and a derivation of the phonon mediated exciton-polariton rate equation used in the kinetic model.

Acknowledgement

This work was supported as part of the the Center for Molecular Quantum Transduction, an Energy Frontier Research Center funded by the U.S. Department of Energy, Office of Science, Basic Energy Sciences under Award #DE-SC0021314. This work made use of the BioCryo facility of Northwestern University's NUANCE Center, which has received support from the SHyNE Resource (NSF ECCS-2025633), the IIN, and Northwestern's MRSEC program (NSF DMR-2308691). This material is based upon work supported by the National Science Foundation Graduate Research Fellowship under Grant No. DGE-2234667.

Competing interests

The authors declare no competing interests.

References

(1) Hümmer, T.; García-Vidal, F. J.; Martín-Moreno, L.; Zueco, D. Weak and strong coupling regimes in plasmonic QED. *Phys. Rev. B.* **2013**, *87*, 1–16.

(2) Carlson, C.; Salzwedel, R.; Selig, M.; Knorr, A.; Hughes, S. Strong coupling regime and hybrid quasinormal modes from a single plasmonic resonator coupled to a transition metal dichalcogenide monolayer. *Phys. Rev. B* **2021**, *104*, 125424.

(3) Ebbesen, T. W. Hybrid Light-Matter States in a Molecular and Material Science Perspective. *Acc. Chem. Res.* **2016**, *49*, 2403–2412.

(4) Ribeiro, R. F.; Martínez-Martínez, L. A.; Du, M.; Campos-Gonzalez-Angulo, J.; Yuen-Zhou, J. Polariton chemistry: controlling molecular dynamics with optical cavities. *Chem. Sci.* **2018**, *9*, 6325–6339.

(5) Nagarajan, K.; Thomas, A.; Ebbesen, T. W. Chemistry under Vibrational Strong Coupling. *J. Am. Chem. Soc.* **2021**, *143*, 16877–16889.

(6) Zeng, H.; Pérez-Sánchez, J. B.; Eckdahl, C. T.; Liu, P.; Chang, W. J.; Weiss, E. A.; Kalow, J. A.; Yuen-Zhou, J.; Stern, N. P. Control of photoswitching kinetics with strong light–matter coupling in a cavity. *J. Am. Chem. Soc.* **2023**, *145*, 19655–19661.

(7) Kasprzak, J.; Richard, M.; Kundermann, S.; Baas, A.; Jeambrun, P.; Keeling, J. M.; Marchetti, F. M.; Szymánska, M. H.; André, R.; Staehli, J. L.; Savona, V.; Littlewood, P. B.; Deveaud, B.; Dang, L. S. Bose-Einstein condensation of exciton polaritons. *Nature* **2006**, *443*, 409–414.

(8) Balili, R.; Hartwell, V.; Snoke, D.; Pfeiffer, L.; West, K. Bose-Einstein Condensation of Microcavity Polaritons in a Trap. *Science* **2007**, *316*, 1007–1010.

(9) Byrnes, T.; Kim, N. Y.; Yamamoto, Y. Exciton–polariton condensates. *Nat. Phys.* **2014**, *10*, 803–813.

(10) Imamoglu, A.; Ram, R. J.; Pau, S.; Yamamoto, Y. Nonequilibrium condensates and lasers without inversion: Exciton-polariton lasers. *Phys. Rev. A* **1996**, *53*, 4250–4253.

(11) Malpuech, G.; Di Carlo, A.; Kavokin, A.; Baumberg, J. J.; Zamfirescu, M.; Lugli, P. Room-temperature polariton lasers based on GaN microcavities. *Appl. Phys. Lett.* **2002**, *81*, 412–414.

(12) Christopoulos, S.; Von Högersthal, G. B. H.; Grundy, A. J.; Lagoudakis, P. G.; Kavokin, A. V.; Baumberg, J. J.; Christmann, G.; Butté, R.; Feltin, E.; Carlin, J. F.; Grandjean, N. Room-temperature polariton lasing in semiconductor microcavities. *Phys. Rev. Lett.* **2007**, *98*, 1–4.

(13) Ramezani, M.; Halpin, A.; Fernández-Domínguez, A. I.; Feist, J.; Rodriguez, S. R.-K.; Garcia-Vidal, F. J.; Gómez Rivas, J. Plasmon-exciton-polariton lasing. *Optica* **2017**, *4*, 31.

(14) Demirchyan, S. S.; Chestnov, I. Y.; Alodjants, A. P.; Glazov, M. M.; Kavokin, A. V. Qubits based on polariton rabi oscillators. *Phys. Rev. Lett.* **2014**, *112*, 1–5.

(15) Pellizzari, T.; Gardiner, S. A.; Cirac, J. I.; Zoller, P. Decoherence, continuous observation, and quantum computing: A cavity QED model. *Phys. Rev. Lett,* **1995**, *75*, 3788–3791.

(16) Cirac, J. I.; Zoller, P.; Kimble, H. J.; Mabuchi, H. Quantum State Transfer and Entanglement Distribution among Distant Nodes in a Quantum Network. *Phys. Rev. Lett.* **1997**, *78*, 3221–3224.

(17) Fleischhauer, M.; Lukin, M. D. Quantum memory for photons: Dark-state polaritons. *Phys. Rev. A.* **2002**, *65*, 1–12.

(18) Kristensen, P. T.; Hughes, S. Modes and Mode Volumes of Leaky Optical Cavities and Plasmonic Nanoresonators. *ACS Photonics* **2014**, *1*, 2–10.

(19) Wang, F.; Christiansen, R. E.; Yu, Y.; Mørk, J.; Sigmund, O. Maximizing the quality factor to mode volume ratio for ultra-small photonic crystal cavities. *Appl. Phys. Lett.* **2018**, *113*.

(20) Reithmaier, J. P.; Sk, G.; Löffler, A.; Hofmann, C.; Kuhn, S.; Reitzenstein, S.; Keldysh, L. V.; Kulakovskii, V. D.; Reinecke, T. L.; Forchel, A. Strong coupling in a single quantum dot-semiconductor microcavity system. *Nature* **2004**, *432*, 197–200.

(21) Yoshie, T.; Scherer, A.; Hendrickson, J.; Khitrova, G.; Gibbs, H. M.; Rupper, G.; Ell, C.; Shchekin, O. B.; Deppe, D. G. Vacuum Rabi splitting with a single quantum dot in a photonic crystal nanocavity. *Nature* **2004**, *432*, 200–203.

(22) Scholes, G. D. Emergence of Collective Coherent States from Strong-Light Coupling of Disordered Systems. *J. Phys. Chem. A* **2021**, *125*, 6739–6750.

(23) Engelhardt, G.; Cao, J. Unusual dynamical properties of disordered polaritons in microcavities. *Phys. Rev. B* **2022**, *105*, 1–19.

(24) Scholes, G. D. Polaritons and excitons: Hamiltonian design for enhanced coherence: Hamiltonian Design for Coherence. *Proc. Math. Phys. Eng. Sci.* **2020**, *476*.

(25) Pérez-Sánchez, J. B.; Koner, A.; Stern, N. P.; Yuen-Zhou, J. Simulating molecular polaritons in the collective regime using few-molecule models. *Proc. Natl. Acad. Sci. U.S.A.* **2023**, *120*, e2219223120.

(26) Thomas, A.; Lethuillier-Karl, L.; Nagarajan, K.; Vergauwe, R. M. A.; George, J.; Chervy, T.; Shalabney, A.; Devaux, E.; Genet, C.; Moran, J.; Ebbesen, T. W. Tilting a ground-state reactivity landscape by vibrational strong coupling. *Science* **2019**, *363*, 615–619.

(27) Xiang, B.; Ribeiro, R. F.; Chen, L.; Wang, J.; Du, M.; Yuen-Zhou, J.; Xiong, W. State-

Selective Polariton to Dark State Relaxation Dynamics. *J. Phys. Chem. A* **2019**, *123*, 5918–5927.

(28) Xiong, W. *Emerging Trends in Chemical Applications of Lasers*; ACS Symposium Series; American Chemical Society, 2021; Vol. 1398; pp 5–89.

(29) Michetti, P.; La Rocca, G. C. Exciton-phonon scattering and photoexcitation dynamics in J-aggregate microcavities. *Phys. Rev. B.* **2009**, *79*, 1–6.

(30) Vasa, P.; Pomraenke, R.; Cirmi, G.; De Re, E.; Wang, W.; Schwieger, S.; Leipold, D.; Runge, E.; Cerullo, G.; Lienau, C. Ultrafast manipulation of strong coupling in metal-molecular aggregate hybrid nanostructures. *ACS Nano* **2010**, *4*, 7559–7565.

(31) Qiu, L.; Mandal, A.; Morshed, O.; Meidenbauer, M. T.; Girten, W.; Huo, P.; Vamivakas, A. N.; Krauss, T. D. Molecular Polaritons Generated from Strong Coupling between CdSe Nanoplatelets and a Dielectric Optical Cavity. *J. Phys. Chem. Lett.* **2021**, *12*, 5030–5038.

(32) Morshed, O.; Amin, M.; Collison, R.; Cogan, N. M.; Koessler, E. R.; Tumiel, T. M.; Girten, W.; Awan, F.; Mathis, L.; Huo, P.; others Room-Temperature Strong Coupling between CdSe Nanoplatelets and a Metal-DBR Fabry–Pérot Cavity. *ChemRxiv* **2023**, DOI:10.26434/chemrxiv–2023–9kllm.

(33) Flatten, L. C.; Christodoulou, S.; Patel, R. K.; Buccheri, A.; Coles, D. M.; Reid, B. P.; Taylor, R. A.; Moreels, I.; Smith, J. M. Strong Exciton-Photon Coupling with Colloidal Nanoplatelets in an Open Microcavity. *Nano Lett.* **2016**, *16*, 7137–7141.

(34) Winkler, J. M.; Rabouw, F. T.; Rossinelli, A. A.; Jayanti, S. V.; McPeak, K. M.; Kim, D. K.; Le Feber, B.; Prins, F.; Norris, D. J. Room-Temperature Strong Coupling of CdSe Nanoplatelets and Plasmonic Hole Arrays. *Nano Lett.* **2019**, *19*, 108–115.

(35) Shlesinger, I.; Monin, H.; Moreau, J.; Hugonin, J. P.; Dufour, M.; Ithurria, S.; Vest, B.; Greffet, J. J. Strong Coupling of Nanoplatelets and Surface Plasmons on a Gold Surface. *ACS Photonics* **2019**, *6*, 2643–2648.

(36) Xia, K.; Sardi, F.; Sauerzapf, C.; Kornher, T.; Becker, H.-W.; Kis, Z.; Kovacs, L.; Dertli, D.; Foglszinger, J.; Kolesov, R.; Wrachtrup, J. Tunable microcavities coupled to rare-earth quantum emitters. *Optica* **2022**, *9*, 445–450.

(37) Botzung, T.; Hagenmüller, D.; Schütz, S.; Dubail, J.; Pupillo, G.; Schachenmayer, J. Dark state semilocalization of quantum emitters in a cavity. *Phys. Rev. B* **2020**, *102*, 144202.

(38) Vanorman, Z. A.; Bieber, A. S.; Wieghold, S.; Nienhaus, L. Green-to-Blue Triplet Fusion Upconversion Sensitized by Anisotropic CdSe Nanoplatelets. *Chem. Mater.* **2020**, *32*, 4734–4742.

(39) Momper, R.; Zhang, H.; Chen, S.; Halim, H.; Johannes, E.; Yordanov, S.; Braga, D.; Blülle, B.; Doblas, D.; Kraus, T.; Kraus, T.; Bonn, M.; Wang, H. I.; Riedinger, A. Kinetic Control over Self-Assembly of Semiconductor Nanoplatelets. *Nano Lett.* **2020**, *20*, 4102–4110.

(40) Scott, R.; Heckmann, J.; Prudnikau, A. V.; Antanovich, A.; Mikhailov, A.; Owschimikow, N.; Artemyev, M.; Climente, J. I.; Woggon, U.; Grosse, N. B.; Achtstein, A. W. Directed emission of CdSe nanoplatelets originating from strongly anisotropic 2D electronic structure. *Nat. Nanotechnol.* **2017**, *12*, 1155–1160.

(41) Lin, C.; Kelley, D. F.; Rico, M.; Kelley, A. M. The "Surface Optical" Phonon in CdSe Nanocrystals. *ACS Nano* **2014**, *8*, 3928–3938.

(42) Maddux, C. J.; Kelley, D. F.; Kelley, A. M. Weak exciton–phonon coupling in CdSe nanoplatelets from quantitative resonance raman intensity analysis. *J. Phys. Chem. C* **2018**, *122*, 27100–27106.

(43) Sun, X.; Geva, E. Non-Condon equilibrium Fermi's golden rule electronic transition rate constants via the linearized semiclassical method. *J. Chem. Phys.* **2016**, *144*, 244105.

(44) Provazza, J.; Tempelaar, R.; Coker, D. F. Analytic and numerical vibronic spectra from quasi-classical trajectory ensembles. *J. Chem. Phys.* **2021**, *155*.

(45) Provazza, J.; Tempelaar, R. Perturbation theory under the truncated Wigner approximation reveals how system-environment entanglement formation drives quantum decoherence. *Phys. Rev. A* **2022**, *106*, 42406.

(46) Herrera, F.; Spano, F. C. Absorption and photoluminescence in organic cavity QED. *Phys. Rev. A* **2017**, *95*, 053867.

(47) Jayaprakash, R.; Kalaitzakis, F. G.; Christmann, G.; Tsagaraki, K.; Hocevar, M.; Gayral, B.; Monroy, E.; Pelekanos, N. T. Ultra-low threshold polariton lasing at room temperature in a GaN membrane microcavity with a zero-dimensional trap. *Sci. Rep.* **2017**, *7*, 1–9.

(48) Amin, M.; Koessler, E. R.; Morshed, O.; Awan, F.; Cogan, N. M.; Collison, R.; Girten, W.; Leiter, C. S.; Vamivakas, A. N.; Huo, P.; others Long-Lived Dynamics Enables Exciton-Polariton Upconversion in CdSe Nanoplatelets. *ChemRxiv* **2023**, DOI:10.26434/chemrxiv–2023–4tshv.

(49) Kéna-Cohen, S.; Forrest, S. R. Room-temperature polariton lasing in an organic single-crystal microcavity. *Nat. Photonics* **2010**, *4*, 371–375.

(50) Pannir-Sivajothi, S.; Campos-Gonzalez-Angulo, J. A.; Martínez-Martínez, L. A.; Sinha, S.; Yuen-Zhou, J. Driving chemical reactions with polariton condensates. *Nat. Commun.* **2022**, *13*, 1–9.